Si Shu, Yun-Fei Jian, Tong Zhang, Wen-Long Guo and Xi Liu*

A novel three-dimensional copper aspartate coordination compound with efficient photoluminescence

https://doi.org/10.1515/znb-2019-0156
Received October 3, 2019; accepted January 6, 2020

Abstract: Solvothermal reaction of a copper salt, racemic aspartic acid ($AspH_3$), and 1,2,4-triazole (TaH) leads to a nanoporous copper aspartate, $Cu_4(Asp)_2(Ta)_2(H_2O)_2 \cdot 2H_2O$ (**1**). The compound was characterized by FT-IR spectroscopy and elemental analysis, and the structure was determined by single-crystal X-ray diffraction. Pairs of L-Asp^{3-} and D-Asp^{3-} ligands in unprecedented μ_4-1,2κO:3,4κOκN coordination modes chelate pairs of adjacent copper cations to form a centrosymmetric 8*n*-membered rectangular pipe, and these pipes are further bridged by copper cations in four directions of the *bc* plane to form a 3D porous structure with approximately rectangular channels of ~5×10 Å^2 along the crystallographic *a*-axis. Along the corners of the rectangular channels, each Ta^- ligand connects three adjacent copper cations in a μ_3 coordination mode to form the final 3D porous framework with relatively large rectangular channels of ~2×8 Å^2 along the *a*-axis. Water molecules reside in these large channels. The thermal stability and solid-state photoluminescence properties of the title compound are also investigated.

Keywords: coordination compound; copper aspartate; crystal structure; metal-organic framework; photoluminescence.

1 Introduction

Metal-organic frameworks (MOFs) built from metal-based nodes and organic linkers have attracted considerable attention in recent years due to their diverse potential applications in a wide range of fields including gas storage/separation, molecular adsorption/separation, drug loading/delivery, catalysis, nonlinear optics, electronics, and sensors [1–5]. Although great efforts have been put into the design and construction of MOFs, controlling the structures as well as regulating the functions of MOFs still remains a challenge because the design and synthesis of MOFs are influenced by many factors, such as the nature of the metal ions, organic ligands, and solvents, as well as the temperature and pH value [6, 7]. The existing protocols have proven that reasonable selection of organic linkers is essential for the construction and control of properties of MOFs [8, 9]. Among the various organic linkers, amino acids have been widely used in the preparation of MOFs since they have multiple binding sites and versatile bonding modes provided by amino and carboxylate groups [10]. Furthermore, the introduction of amino acid moieties in MOFs may induce the intrinsic chirality of the starting amino acids in extended structures [11].

Aspartic acid ($AspH_3$) is an acidic amino acid with one amine and two carboxylic acid groups. Since each of these functional groups is capable of binding to metal centers, the aspartate anion has a variety of coordination modes [10]. This polyfunctionality makes it a suitable organic linker for the construction of MOFs. According to a survey of the Cambridge Structural Database (CSD V5.38 updated August 2018), MOFs based on metal aspartates typically feature a tridentate chelation to a central metal ion comprised of a five-membered and a six-membered N,O-chelation motifs. They generally exhibit one-dimensional (1D) structures linked by an oxygen atom of the terminal carboxylate group involved in the six-membered chelation [12–14], but seldom display as three-dimensional (3D) dense structures with solvent-accessible volume [10, 15]. In all reported MOFs based on metal aspartates, the amino group ($-NH_2$) of $AspH_3$ exists only in one conformation within each structure and coordinates to only one metal cation. In the work described in this paper, $AspH_3$ was selected to react with a copper(II) salt and 1,2,4-triazole under solvothermal condition to give a new 3D nanoporous MOF, namely, $Cu_4(Asp)_2(Ta)_2(H_2O)_2 \cdot 2H_2O$ (**1**). In this compound, each of the Asp^{3-} ligands displays an

***Corresponding author: Xi Liu,** Chongqing Key Laboratory of Green Synthesis and Applications, College of Chemistry, Chongqing Normal University, Chongqing 401331, P.R. China, e-mail: xliu@cqnu.edu.cn
Si Shu, Yun-Fei Jian, Tong Zhang and Wen-Long Guo: Chongqing Key Laboratory of Green Synthesis and Applications, College of Chemistry, Chongqing Normal University, Chongqing 401331, P.R. China

unprecedented coordination mode of μ_4-1,2κO:3,4κOκN. The synthesis, crystal structure, thermal stability, and solid-state photoluminescence of the compound were investigated.

2 Results and discussion

2.1 Crystal structure analysis

Single-crystal X-ray diffraction analysis has revealed that MOF **1** crystallizes in the monoclinic space group $P2_1/c$. The asymmetric unit contains four unique Cu(II) cations, two Asp^{3-} ligands, two Ta^- ligands, two coordinated water molecules, and two water guest molecules. As shown in Fig. 1, the Cu1 cation is located in a distorted square-pyramidal geometry formed by two N atoms from two Ta^- ligands, one carboxylate O atom and one amino N atom from an Asp^{3-} ligand, and one coordinated aqua O atom. The Cu2 cation also lies in a distorted square-pyramidal coordination environment and is coordinated by one N atom from a Ta^- ligand, two carboxylate O atoms from two Asp^{3-} ligands, and one carboxylate O atom and one N atom from one Asp^{3-} ligand. The Cu3 cation is situated in a distorted square-pyramidal geometry formed by two N atoms from two Ta^- ligands, one carboxylate O atom and one N atom from one Asp^{3-} ligand, and one carboxylate O atom from another Asp^{3-} ligand, while the Cu4 cation is also seated in a distorted square-pyramidal coordination environment and is coordinated by one carboxylate O atom and one amino N atom from one Asp^{3-} ligand, and one carboxylate O atom from another Asp^{3-} ligand, one N atom from a Ta^- ligand, and one aqua O atom. Although the four crystallographically unique Cu(II) cations are located in similar square-pyramidal coordination environments, the detailed components of the coordination geometries are very different. Each of the two Ta^- ligands has a μ_3-1,2,3κN coordination mode, which is a common pattern for a 1,2,4-triazole ligand. Each of the two Asp^{3-} ligands adopts an unprecedented coordination mode of μ_4-1,2κO:3,4κOκN and exhibits a tridentate chelation to two adjacent metal cations with the formation of two metallacycles. One originates from the five-membered N,O-chelate motif, which is prevalent in amino acid coordination chemistry, while the other is a six-membered N,O chelation from the carboxylate side chain of the Asp^{3-} ligand. It should be noted that aspartic acid usually loses two carboxylic hydrogen atoms to form an $AspH^{2-}$ ligand when it binds to metal ions, whereas in the title compound it loses two carboxylic hydrogen atoms and one amino hydrogen atom to become an Asp^{3-} ligand, which has not been reported according to the survey of the Cambridge Structural Database (CSD V5.38 updated August 2018).

Two pairs of L-Asp^{3-} and D-Asp^{3-} ligands chelate two pairs of adjacent Cu2 and Cu4 cations to form a centrosymmetric eight-membered ring. These eight-membered rings are further connected to each other by the carboxylate group of the Asp^{3-} ligands to form a centrosymmetric 8*n*-membered rectangular pipe with the effective size

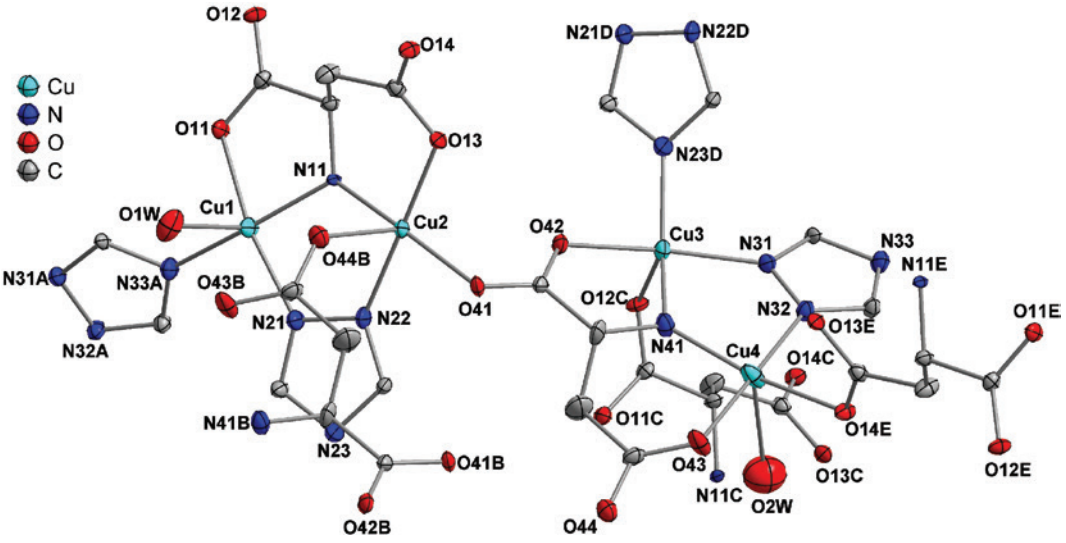

Fig. 1: Coordination environments of the Cu(II) cations in **1** (30% probability displacement ellipsoids). All hydrogen atoms and water guest molecules are omitted for clarity. Symmetry codes A: 1+*x*, 0.5 – *y*, –0.5+*z*; B: 1 – *x*, –*y*, 1 – *z*; C: *x*, 0.5 – *y*, 0.5+*z*; D: –1+*x*, *y*, *z*, 2 – *z*; E: –*x*, –*y*, 1 – *z*.

of ~2×3 Å^2 along the crystallographic *a*-axis (Fig. 2a). The 8*n*-membered rectangular pipes are further bridged by Cu1 and Cu3 cations in four directions of the *bc* plane to form a 3D porous structure with approximately rectangular channels of ~5×10 Å^2 along the *a*-axis (Fig. 2b and c). Along the corners of the rectangular channels, each of the Ta$^-$ ligands connects three adjacent Cu(II) cations in a μ_3-1,2,3κN coordination mode to form the 3D porous framework with relatively large rectangular channels of ~2×8 Å^2 along the *a*-axis (Fig. 2d and e). Water guest molecules reside in these large channels. By using the routine SOLV of PLATON [16], the accessible voids in the desolvated structure of **1** are estimated as 463.6 Å^3 per unit cell volume of 2380.0 Å^3 (calcd: 19.5%). In addition, there are abundant, strong classical N–H···O, O–H···O, and O–H···N hydrogen bonds (Table S3) among the coordinated water molecules, guest water molecules, and imido groups of the Asp^{3-} ligands, which stabilize the final 3D porous

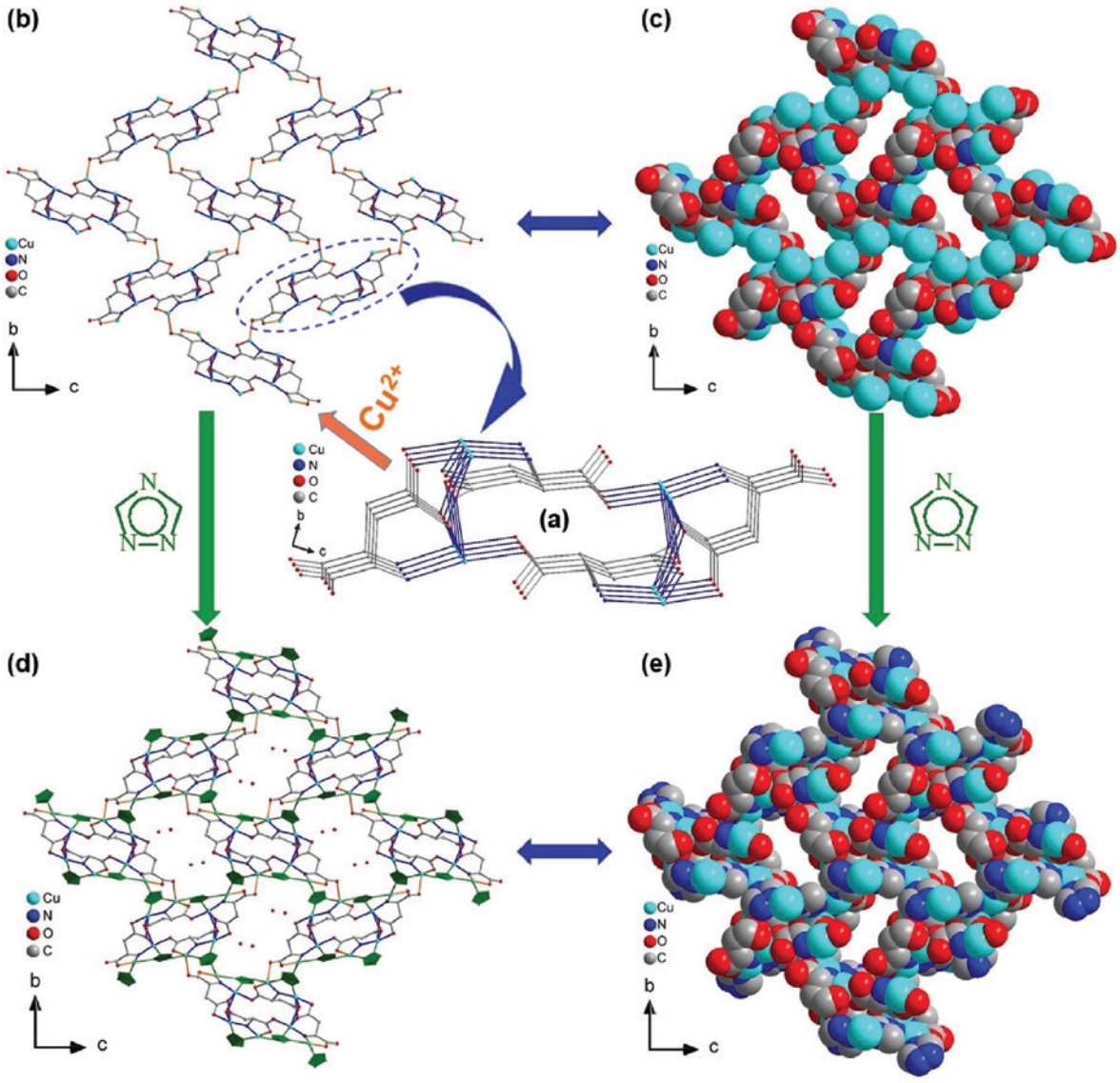

Fig. 2: Details of the molecular and crystal structure of **1:** (a) Pairs of L-Asp^{3-} and D-Asp^{3-} ligands connect (blue bonds) the Cu2 and Cu4 cations to form a centrosymmetric 8*n*-membered rectangular pipe along the *a*-axis. (b) The 8*n*-membered rectangular pipes further bridge (orange bonds) the Cu1 and Cu3 cations in four directions of the *bc* plane to form a 3D porous structure with approximately rectangular channels along the *a*-axis. (c) Space-filling representation of the 3D porous structure along the *a*-axis. (d) Along the corners of the rectangular channels, each of the Ta$^-$ ligands (represented as green five-membered ring plane) connects (green bonds) three adjacent Cu(II) cations in a μ_3 coordination mode to form a 3D porous framework with approximately rectangular channels of ~2×8 Å^2 along the *a*-axis. Water guest molecules reside in these channels. (e) Space-filling representation of the 3D porous framework along the *a*-axis. Hydrogen atoms and water guest molecules (except for (d)) are omitted for clarity.

framework. Interestingly, a Cu(II) complex with similar structure, $Cu_4(Trz)_2(Mal)_2(H_2O)_2 \cdot 3H_2O$ (TrzH = 1,2,4-triazole, $MalH_3$ = malic acid), has been reported recently [17]. The compound is built up from the deprotonated malic acid (Mal^{3-}: $C_4H_3O_5$) and 1,2,4-triazole ligands, while MOF **1** is constructed from deprotonated aspartic acid (Asp^{3-}: $C_4H_4NO_4$) and 1,2,4-triazole ligands. In the two compounds, the malic acid ligand (Mal^{3-}) and aspartic acid ligand (Asp^{3-}) adopt similar coordination modes (μ_4-1,2κO:3,4κOκO vs. μ_4-1,2κO:3,4κOκN) and similar structural configurations, although they have different functional groups (–OH vs. $-NH_2$).

2.2 Powder X-ray diffraction

A powder X-ray diffraction (PXRD) experiment was carried out to confirm that the phase of the bulk sample was pure and the crystal structure of **1** is truly representative of the bulk material. As shown in Fig. 3, the major peak positions of the PXRD patterns of the bulk sample are in good agreement with those of the corresponding simulated ones obtained from the single-crystal data, indicating the presence of one main crystalline phase, and that the single crystal is identical with the synthesized bulk material.

2.3 Thermogravimetric analysis

The thermal decomposition behavior of **1** was investigated under an air atmosphere in order to characterize its thermal stability. As displayed in Fig. 4, the first continuous weight loss of 10.8% in the temperature range

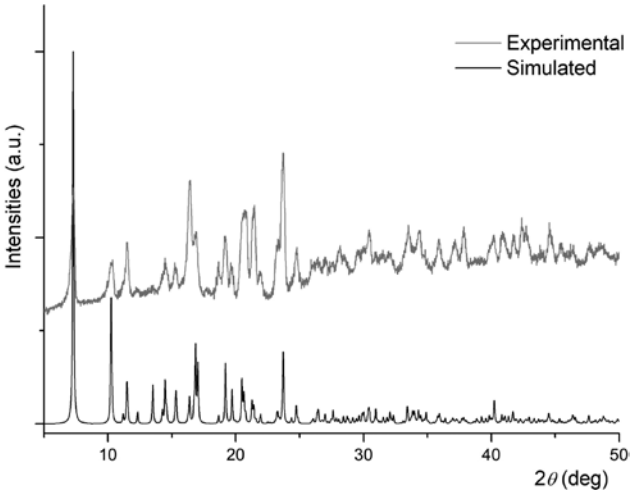

Fig. 3: Measured and simulated PXRD patterns of **1**.

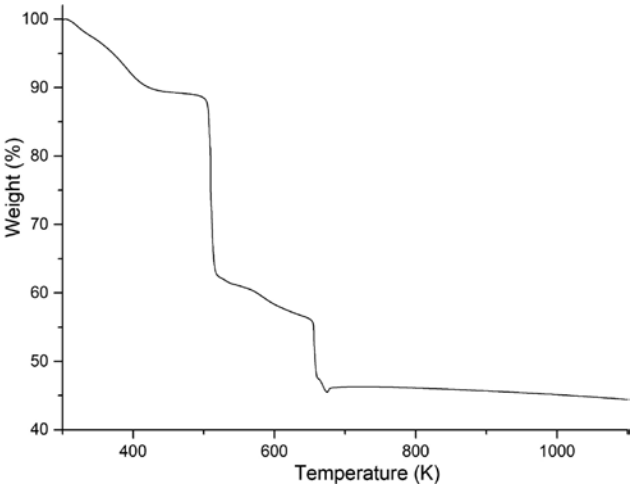

Fig. 4: Thermogravimetric analysis (TGA) curve of **1**.

T = 303–503 K corresponds to the loss of free and coordinated water molecules (calculated as 10.0% for two coordinated water and two free water molecules per formula unit). The residual framework continues to decompose with complicated weight losses up to about 674 K. The observed final mass remnant of 45.4% likely represents CuO, in agreement with the calculated value of 44.0%.

2.4 Photoluminescence behavior

Solid-state luminescence spectra show that MOF **1** exhibits four relatively strong emission peaks around 404, 423, 462, and 482 nm upon maximum photoexcitation at 298 nm, and the free TaH ligand displays three relatively strong emission bands around 398, 419, and 460 nm upon maximum excitation at 252 nm, while the free $AspH_3$ ligand shows three relatively weak emission peaks around 420, 460, and 484 nm upon excitation at 298 nm (Fig. 5). In comparison with those of the free TaH and $AspH_3$ ligands, the emission bands of **1** display small shifts (within 6 nm) with similar band shapes and slightly wider spectral ranges, as well as significantly enhanced emission intensities. In detail, complex **1** and the free TaH ligand have three similar pairs of emissions, 404 vs. 398, 423 vs. 419, and 462 vs. 460 nm, while for **1** and $AspH_3$ there are also three similar pairs of emissions, 423 vs. 420, 462 vs. 460, and 482 vs. 484 nm. The largest shift within corresponding emission pairs is about 6 nm (404 vs. 398 nm). Each pair of emission may be originating from the same emission process.

The small shifts and similar band shapes may suggest that the emissions of MOF **1** probably originate from the TaH and $AspH_3$ ligands, i.e. MOF **1** is probably subject to an intra-ligand charge transfer (ILCT) processes. The

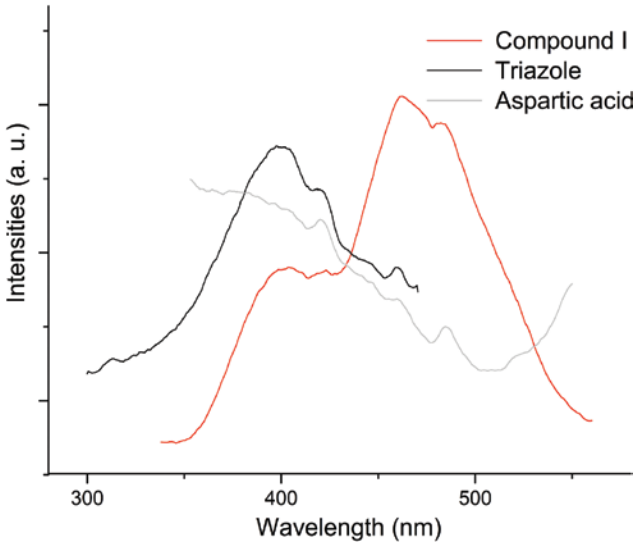

Fig. 5: Solid-state photoluminescence emission spectra of **1**, TaH, and $AspH_3$ ligands upon photoexcitation at 298 or 252 nm at room temperature.

intensity difference of the emission bands may be due to the conjugation effect of the Cu ions and the Ta^- and Asp^{3-} ligands. The coordination interactions between metal ions and organic ligands usually enhance the rigidity of the ligands, resulting in stronger luminescence intensity of the compounds [18].

3 Conclusion

In summary, we have synthesized a novel photoluminescent copper aspartate compound in which the Asp^{3-} ligand displays the unprecedented coordination mode μ_4-1,2κO:3,4κOκN. The synthesis strategy used for the compound may be expanded to prepare other aspartate complexes [19] of transition metals having this special coordination mode. Further experiments based on this idea are under way.

4 Experimental

4.1 Materials and instrumentation

All chemicals were obtained from commercial sources and were used without further purification. The FT-IR spectra were recorded from KBr pellets on an FT-IR 8400S (CE) instrument in the range 4000–400 cm^{-1}. C, H, and N elemental analyses were carried out on a Vario EL III elemental analyzer. X-ray powder diffraction data were recorded with CuK_α radiation ($\lambda = 1.5406$ Å) on an XRD-6100 apparatus with a scan speed of 2 o min^{-1}. Thermogravimetric analyses were performed on a HENVEN-HJ HCT-3 thermoanalyzer at a heating rate of 10 K min^{-1} under air atmosphere. Photoluminescence analyses were carried out on a Perkin-Elmer LS55 fluorescence spectrometer.

4.2 Synthesis of complex 1

A mixture of $Cu(NO_3)_2 \cdot 3H_2O$ (241.6 mg, 1.0 mmol), D- $AspH_3$ 34.6 mg, 0.5 mmol), and L-$AspH_3$ (34.6 mg, 0.5 mmol) was added to a mixed solvent of ethanol/H_2O (volume ratio 1:3.8 mL), and then 5 µL of a 6M NaOH solution was added to adjust the pH value of the solution to ~10. The resulting aqueous solution was transferred into a 25-mL Teflon-lined stainless steel reactor and kept at $T = 413$ K for 3 days, and then slowly cooled to room temperature at a rate of 10 K h^{-1}. Blue block crystals of **1** were obtained in 60% yield (about 217 mg) based on the H_3Asp ligand. Analysis calculated (%) for $C_{12}H_{20}Cu_4N_8O_{12}$ $(Cu_4(Asp)_2(Ta)_2(H_2O)_2 \cdot 2H_2O)$: C 19.95, H 2.79, N 15.51; Found C 20.03, H 2.86, N 15.47. FT-IR (KBr, 4000–400 cm^{-1}): $\nu = 3421$(br, w), 1574(s), 1547(s), 1520(s), 1435(w), 1393(s), 1309(w), 1292(w), 1171(m), 1119(w), 1092(s), 1003(w), 978(w), 906(m), 824(w), 721(m), 663(m), 611(w), 575(w) cm^{-1}.

Additional remark: MOF **1** was originally synthesized using enantiopure L-$AspH_3$ under similar reaction conditions. The racemic character of **1** probably results from the partial configuration transformation of L-$AspH_3$ to D-$AspH_3$ under the applied solvothermal reaction conditions. In particular, the pH value (strongly alkaline conditions) has been shown to be an important factor leading to the racemization of natural amino acids [19] in the presence of metal ions and hence to the synthesis of **1** in our case.

4.3 X-ray single-crystal structure determination of 1

A suitable single crystal of **1** was carefully selected under an optical microscope and glued to a thin glass fiber. The data collection was performed on a Rigaku Mercury CCD diffractometer equipped with graphite-monochromatized Mo$K\alpha$ radiation ($\lambda = 0.71073$ Å) at $T = 293$ K. The intensity dataset was collected with ω-scan technique and reduced by CrystalClear V1.35 software [20]. The structure was solved by Direct Methods and refined by full-matrix least-squares techniques. Non-hydrogen atoms were located by difference Fourier maps and subjected to anisotropic

refinement. Water H atoms were located from a difference Fourier map and refined with the O–H bond length restrained to 0.85 Å and assigned isotropic displacement parameters of $U_{iso}(H) = 1.5U_{eq}(O)$. All carbon H atoms were allowed to ride on their respective parent C atoms with C–H distances of 0.93 or 0.97 Å, and were included in the structure factor calculations with assigned isotropic displacement parameters of $U_{iso}(H) = 1.2U_{eq}(C)$. Three reflections, which are rather large outliers in the refinement, namely 002, 020, and $\bar{1}13$, were excluded from the final refinement cycles. The O2W, O3W, O4W, and N41 atoms have big average residual U_{eq} values due to the large thermal vibrations of the guest water molecules, and ISOR instructions were applied to the four atoms which led to 18 restraints. All calculations were performed with the Siemens SHELXTL (version 5) crystallographic software [21–23].

Crystallographic Data for ***1*****:** $C_{12}H_{20}Cu_4N_8O_{12}$, $M_r = 722.52$, crystal size: $0.35 \times 0.07 \times 0.07$ mm^3, monoclinic, space group, $P2_1/c$, $a = 8.0789$ (5), $b = 17.0871$ (6), $c = 17.6377$ (6) Å, $\beta = 102.180$ (2)°, $V = 2379.99$ (19) Å^3, $T = 296(2)$ K, $Z = 4$, $D_{calcd} = 2.02$ g cm^{-3}, $\mu = 3.6$ mm^{-1}, $F(000) = 1440$ *e*; 22,095 reflections measured in the range $2.661 < \theta < 25.500°$, 4419 unique ($R_{int} = 0.0482$). Structure solution and refinement based on 3758 observed reflections with $I > 2\sigma(I)$ and 325 refined parameters and 18 restraints gave $R1 = 0.0684$, $wR2 = 0.1933$ and $S = 1.001$ and $R1 = 0.0807$, $wR2 = 0.2060$, and $S = 1.010$ for all reflections; $\Delta\rho_{fin}$ (max/min) = 2.49/ – 2.13 *e* Å^{-3}.

CCDC 1952090 contains the supplementary crystallographic data for this paper. These data can be obtained free of charge from The Cambridge Crystallographic Data Centre via www.ccdc.cam.ac.uk/data_request/cif.

5 Supporting information

Further crystal structure data, selected bond lengths and angles, and hydrogen bond distances and angles are given as supplementary material available online (DOI: 10.1515/znb-2019-0156).

Acknowledgment: We gratefully acknowledge financial support of the National Natural Science Foundation of China (21071156) and the Natural Science Foundation of Chongqing (cstc2019jcyj-msxmX0170).

References

[1] A. Dhakshinamoorthy, Z. Li, H. Garcia, *Chem. Soc. Rev.* **2018**, *47*, 8134–8172.
[2] A. Kirchon, L. Feng, H. F. Drake, E. A. Joseph, H. Zhou, *Chem. Soc. Rev.* **2018**, *47*, 8611–8638.
[3] M. J. V. Vleet, T. Weng, X. Li, J. R. Schmidt, *Chem. Rev.* **2018**, *118*, 3681–3721.
[4] Y. Cui, J. Zhang, H. Hea, G. Qian, *Chem. Soc. Rev.* **2018**, *47*, 5740–5785.
[5] H. Wang, W. P. Lustig, J. Li, *Chem. Soc. Rev.* **2018**, *47*, 4729–4756.
[6] Z. Sun, M. Yang, Y. Ma, L. C. Li, *Cryst. Growth Des.* **2017**, *17*, 4326–4335.
[7] S. B. Zhou, X. F. Wang, C. C. Du, D. Z. Wang, D. Z. Jia, *CrystEngComm* **2017**, *91*, 3124–3137.
[8] C. L. Tao, B. C. Chen, X. G. Liu, L. J. Zhou, X. L. Zhu, J. Cao, Z. G. Gu, Z. J. Zhao, L. Shen, B. Z. Tang, *Chem. Commun.* **2017**, *53*, 9975–9978.
[9] N. Bendjellal, C. Trifa, S. Bouacida, C. Boudaren, M. Boudraa, H. Merazig, *Acta Crystallogr.* **2018**, *C74*, 240–247.
[10] J. A. Gould, J. T. A. Jones, J. Bacsa, Y. Z. Khimyak, M. J. Rosseinsky, *Chem. Commun.* **2010**, *46*, 2793–2795.
[11] R. Vaidhyanathan, D. Bradshaw, J. N. Rebilly, J. P. Barrio, J. A. Gould, N. G. Berry, M. J. Rosseinsky, *Angew. Chem. Int. Ed.* **2006**, *45*, 6495–6499.
[12] L. Antolini, L. Menabue, G. C. Pellacani, G. Marcotrigiano, *J. Chem. Soc., Dalton Trans.* **1982**, 2541–2543.
[13] R. Calvo, C. A. Steren, O. E. Piro, T. Rojo, F. J. Zuniga, E. E. Castellano, *Inorg. Chem.* **1993**, *32*, 6016–6022.
[14] H. Schmidbaur, I. Bach, J. Riede, G. Müller, J. Helbig, G. Hopf, *Chem. Ber.* **1988**, *121*, 795–797.
[15] E. V. Anokhina, Y. B. Go, Y. Lee, T. Vogt, A. J. Jacobson, *J. Am. Chem. Soc.* **2006**, *128*, 9957–9962.
[16] A. L. Spek, *Acta Crystallogr.* **2009**, *D65*, 148–155.
[17] X. Wang, Y. Zhao, Z. Jagličić, S. Wang, S. Lin, X. Li, D. Sun, *Dalton Trans.* **2015**, *44*, 11013–11020.
[18] Y. L. Wang, L. L. Long, J. F. Zhang, *Acta Crystallogr.* **2015**, *C71*, 435–439.
[19] H. Schmidbaur, H. G. Classen, J. Helbig, *Angew. Chem. Int. Ed. Engl.* **1990**, *29*, 1090–1103.
[20] CRYSTALCLEAR (version 1.35), An Integrated Program for the Collection and Processing of Area Detector Data, Rigaku Corporation, Tokyo (Japan) **2002**.
[21] G. M. Sheldrick, SHELXTL (version 5), Reference Manual, Siemens Analytical X-ray Instruments Inc., Madison, WI (USA) **1994**.
[22] G. M. Sheldrick, *Acta Cryst.* **2015**, *A71*, 3–8.
[23] G. M. Sheldrick, *Acta Cryst.* **2015**, *C71*, 3–8.

Supplementary Material: The online version of this article offers supplementary material (https://doi.org/10.1515/znb-2019-0156).